Article:
Mu, Q, David, CA, Galceran, J et al. (2014) Systematic investigation of the physicochemical factors that contribute to the toxicity of ZnO nanoparticles. Chemical Research in Toxicology, 27 (4). 558 - 567. ISSN: 0893-228X

https://doi.org/10.1021/tx4004243

A systematic investigation of the physico-chemical factors that contribute to the toxicity of ZnO nanoparticles

Qingshan Mu[1,2], *Calin A. David*[3], *Josep Galceran*[*,3], *Carlos Rey-Castro*[3], *Łukasz Krzemiński*[1], *Rachel Wallace*[4], *Faith Bamiduro*[4], *Steven J. Milne*[4], *Nicole S. Hondow*[4], *Rik Brydson*[4], *Gema Vizcay-Barrena*[5], *Michael N. Routledge*[*,2], *Lars J.C. Jeuken*[*,1] *and Andy P. Brown*[*,4]

[1] School of Biomedical Sciences; University of Leeds, LS2 9JT, Leeds, UK

[2] Leeds Institute of Genetics, Health and Therapeutics, School of Medicine; University of Leeds, LS2 9JT, Leeds, UK

[3] Departament de Química and AGROTECNIO, Universitat de Lleida, Rovira Roure 191, 25198 Lleida, Catalonia, Spain

[4] Institute for Materials Research, School of Process, Environmental and Materials Engineering, University of Leeds, LS2 9JT, Leeds, UK

[5] Centre for Ultrastructural Imaging, Kings College London, SE1 1UL, Kings College London, UK

[*] Corresponding author: galceran@quimica.udl.cat

[*] Corresponding author: M.N.Routledge@leeds.ac.uk

[*] Corresponding author: L.J.C.Jeuken@leeds.ac.uk

[*] Corresponding author: A.P.Brown@leeds.ac.uk

Table of Contents Graphic

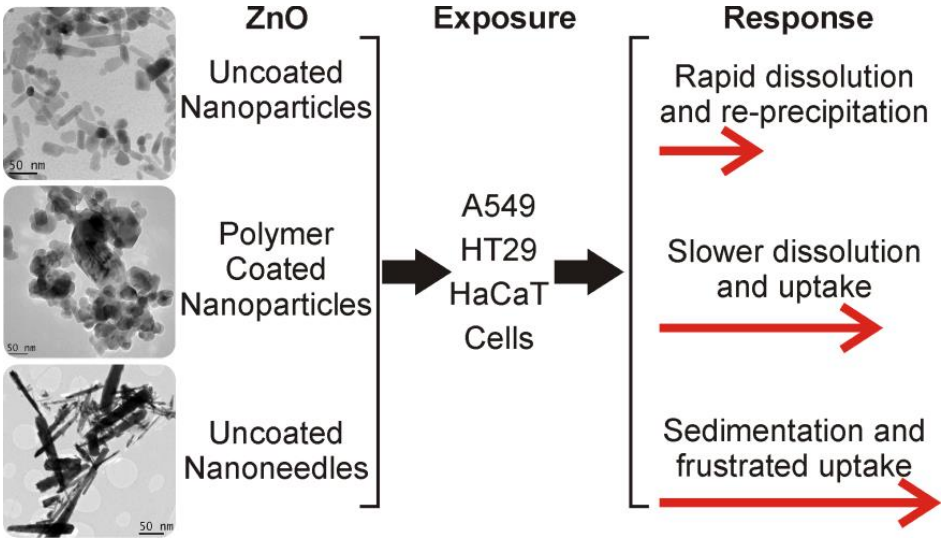

Abstract

ZnO nanoparticles (NPs) are prone to dissolution and uncertainty remains whether biological/cellular responses to ZnO NPs are solely due to the release of Zn^{2+} or whether the NPs themselves have additional toxic effects. We address this by establishing ZnO NP solubility in dispersion media (Dulbecco's Modified Eagle Medium, DMEM) held under identical conditions to those employed for cell culture (37 ^{o}C, 5% CO_2 and pH 7.68) and by systematic comparison of cell-NP interaction for three different ZnO NP preparations. For NPs at concentrations up to 5.5 μg ZnO/mL, dissolution is complete (with the majority of the soluble zinc complexed to dissolved ligands in the medium), taking ca. one hour for uncoated and ca. 6 hours for polymer coated ones. Above 5.5 μg/mL results are consistent with the formation of zinc carbonate, keeping the solubilised zinc fixed to 67 μM of which only 0.45 μM is as free Zn^{2+}, i.e., not complexed to dissolved ligands. At these relatively high concentrations, NPs with an aliphatic polyether-coating show slower dissolution (i.e. slower free Zn^{2+} release) and re-precipitation kinetics compared to uncoated NPs, requiring more than 48 hours to reach thermodynamic equilibrium. Cytotoxicity (MTT) and DNA damage (Comet) assay dose response curves for three epithelial cell lines suggest that dissolution and re-precipitation dominate for uncoated ZnO NPs. Transmission electron microscopy combined with monitoring of intracellular Zn^{2+} concentrations and ZnO-NP interactions with model lipid membranes indicate that an aliphatic polyether-coat on ZnO NPs increases cellular uptake, enhancing toxicity by enabling intracellular dissolution and release of Zn^{2+}. Similarly, we demonstrate that needle-like NP morphologies enhance toxicity by apparently frustrating cellular uptake. To limit toxicity, ZnO NPs with non-acicular morphologies and coatings that only weakly interact with cellular membranes are recommended.

CAS section: Toxicology

Introduction

The widespread use of nanoparticles (NPs) in industry and consumer products has led to an intense research effort into the effects of engineered NPs on human health and the environment. Zinc oxide (ZnO) NPs are one of the materials that have been extensively studied because of their use in cosmetic preparations, especially in sun cream. Recent research has demonstrated that ZnO is likely to dissolve and undergo phase transformations in aqueous environments, typically forming nanoparticulate compounds of lower solubility (zinc-phosphates, -carbonates, -sulphides and/or -iron hydroxides).[1-3] Dissolution of ZnO NPs and the re-precipitation as zinc carbonates and phosphates in different cell culture media has also been suggested; with the phosphate concentration of the media having a major effect on the equilibrium Zn^{2+} levels in solution.[4, 5] As such, a careful assessment of the effect of solution chemistry on the physico-chemical properties of ZnO should be carried out as part of any complete nanotoxicology study.

Since ZnO NPs are prone to dissolution,[2, 6, 7] it has been suggested that the released free Zn^{2+} ions are responsible for the observed toxicity, including damage to DNA via the generation of radical oxygen species (ROS).[8-10] For instance, Song *et al.* showed that the concentration of soluble zinc in the supernatant of a complete cell medium (Roswell Park Memorial Institute, RPMI 1640 medium supplemented with 10% fetal serum albumin) after centrifugation was about 10 μg/mL.[9] They suggested that this zinc fraction is the Zn^{2+} released by dissolution of ZnO NPs and assert that the dissolved Zn^{2+} contributed to about 50% of the observed cell death *in vitro*, where ROS levels in the cell were proposed to be mainly due to a cytotoxic response to Zn^{2+} inside the cell. The difference in toxicity between different ZnO particles was attributed to the non-dissolved particles.[9] Other reports, however, suggest that ROS are generated at the surface of ZnO NPs (e.g., [11]) or that ZnO NPs are directly taken up by cells,

increasing the intracellular Zn^{2+} concentration to toxic levels not achieved by extra cellular exposure to similar concentration of soluble zinc salts.[12-14] This latter effect is supported by a report that direct NP-cell contact is required to generate toxicity within human cancer cells.[15]

Also studies *in vivo* have started to address the role of ZnO dissolution. Cho et al. show that intratracheal instillation of ZnO NPs into the lungs of rats results in rapid pH-dependent dissolution of the ZnO in phagosomes and a toxic response consistent with the release of Zn^{2+}.[16] Sharma *et al.* fed mice 300 mg ZnO/kg for 14 consecutive days and detected an accumulation of Zn^{2+} in the liver, which was associated with significant oxidative stress.[17]

To fully determine toxicity of NPs, it is now well established that *in vitro* toxicity assays need adjustments and that detailed physico-chemical characterisation of the NPs is required to cross-reference results for different sources of NPs.[18-23] Ultimately, the toxicity of engineered NPs in general is dependent on the morphology, size (including hydrodynamic agglomeration state) and coating of the particles.[19] For ZnO NPs, the additional dissolution kinetics are also likely to depend on the morphology, size, hydrodynamic agglomeration and coating of the particles as well as the composition and conditions of the medium the particles are suspended in. As such, it is possible that much of the uncertainty described above regarding the mechanism of ZnO NP toxicity is due to variation in dissolution kinetics.

After an initial cell cytotoxicity screen of six different Zn NPs (Supplementary Information, Figure S1, Table S1) we have undertaken a systematic study of three different ZnO NP types (polymer coated, uncoated equiaxed and needle-like ZnO NPs). Here, we report on the equilibrium dissolution, dissolution rates and re-precipitation of these ZnO NPs in CO_2 buffered cell culture media and go on to compare the cytotoxicity and DNA damage to

investigate the role of released, free Zn^{2+}. We also investigate cellular uptake and interaction with lipid membranes to highlight the role of the less rapidly dissolved NP fraction. The results identify three mechanisms by which ZnO NPs can cause cytotoxicity.

Experimental Procedures

ZnO nanoparticles and characterisation

NP sample 1, EZ-1; commercial, *NanoTek*® NPs were bought via Alfa Aesar (Cat #: 45409; the exact formulation and coating details were unreported). These ZnO NPs have a coating in order to disperse well in liquids; ATR-FTIR indicates the coating to be an aliphatic polyether (Supplementary Information, Figure S2 and S3). NP sample 2, EZ-2; commercial, uncoated NPs were bought from Alfa Aesar (Cat #: 44533). NP sample 3, EZ-3; nano-needles were hydrothermally synthesized from $ZnCl_2$ and Na_2CO_3 dissolved in distilled water (140°C for 12 h). The final precipitates obtained were separated from the liquid phase and washed 6 times with distilled water.

Physico-chemical characterisation

Transmission electron microscopy (TEM) was conducted on an FEI Tecnai F20 FEG-TEM operated at 200 kV and equipped with a Gatan Orius SC600A CCD camera and an Oxford Instruments 80mm X-Max SDD detector. ZnO NPs were prepared for TEM by placing a drop of the NPs suspended in alcohol onto a copper TEM grid coated with a holey carbon support film (Agar Scientific Ltd.) and allowed to air dry before examination in the TEM.

Dynamic Light Scattering (DLS) and Zeta Potential measurements were performed using a Malvern Zetasizer Nano ZS in water and (serum-free) cell culture media. Each sample was analyzed 5 times with the average result presented. Powder X-ray Diffraction (XRD) was

undertaken using a Bruker D8 powder X-ray diffractometer fitted with a Vantec detector and using a Cu-Kα source (1.540 Å). Inductively Coupled Plasma-Mass Spectrometry (ICP-MS) was conducted using a Perkin Elmer Elan DRC-e ICP-MS following centrifugation (for 35 min in an Eppendorf MiniSpin Plus, at 14,500 rpm) and extraction of the supernatant of NP containing solutions. Fourier Transform-Infra Red (FT-IR) spectrometry was conducted on a Thermo Scientific iS10 FTIR spectrometer using an attenuated total reflection (ATR) accessory.

Dissolution assay

Dissolution behaviour of ZnO NPs was investigated using the electro-analytical technique Absence of Gradients and Nernstian Equilibrium Stripping (AGNES),[7, 24] which does not require any prior separation of the dispersed and liquid phases. Stock NP samples were suspended in MilliQ water at 1 mg/mL (or for EZ-1 the as-received colloidal suspension in water at a nominal concentration of 400 mg/mL was used). These were sonicated (Branson 3510E-MT Ultrasound bath, 100 W 42 KHz) for 10 min prior to dispersion at the appropriate concentrations in polarographic cells containing Dulbecco's Modified Eagle Medium (DMEM; Sigma, UK, cat D5796) held at 37.0 ± 0.1 $^{\circ}$C and in 5% CO_2 (± 0.5%) for careful control of pH and temperature. DMEM is buffered with sodium bicarbonate (3.7 g $NaHCO_3$/L), contains only a small amount of phosphate (0.109 g NaH_2PO_4/L) and pH is fixed at 7.68 ± 0.04 throughout the experiment by inclusion of 5% CO_2 in the environment. Dissolution studies were undertaken on EZ-1, EZ-2 and ZnO NPs purchased from Sigma-Aldrich (cat no. 544906). No significant differences were observed between the two uncoated NPs (EZ-2 and Sigma-Aldrich). The latter NPs have been characterised previously[7] and shown to be phase pure by XRD with a primary equiaxed particle morphology ~70 nm in diameter. When dispersed in water they coalesced to agglomerates with a hydrodynamic

diameter of ~140 nm and when dispersed in water plus a background electrolyte (at 0.1 ionic strength) they coalesced to agglomerates with a hydrodynamic diameter of ~1100 nm.

Cell culture, viability and genotoxicity assays

A549 (human lung alveolar carcinoma) cells and HT29 (human colon cancer) cells (Sigma-Aldrich) were cultured in DMEM containing 10% foetal bovine serum (Lonza, Slough, UK) with 0.5% penicillin/streptomycin. HaCaT (human keratinocyte) cells (gifted from within the University of Leeds) were cultured in RPMI media (Gibco, Paisley, Scotland) containing 10% foetal bovine serum (Lonza, Slough, UK) with 0.5% penicillin/streptomycin. All cell lines were incubated at 37° C in humidified 5% CO_2 until they were approaching confluence, when they were harvested using trypsin-ethylenediamine tetra-acetic acid (EDTA) and then re-seeded.

Effects of ZnO NPs on the viability and genetic fidelity of the cells were evaluated using the MTT (thiazolyl blue tetrazolium bromide) and Comet assays, respectively, using a modified protocol to that described previously.[25] Suspensions of EZ-2 and EZ-3 were made in water (1 mg/mL and 10 mg/mL) and bath-sonicated (Decon, FS minor) for 30 min before adding them to the cell media in appropriate concentrations. We note that in this assay the cells have been incubated with ZnO NPs for 24 h in the *absence* of foetal bovine serum. In the MTT assay, light absorption was corrected for dispersion from the ZnO NPs by using transmission intensities from wells containing no cells. For control studies with $ZnSO_4$ (Sigma-Aldrich), the exposure concentrations were adjusted to give the same molar content of elemental Zn as the experiments with ZnO NPs. Cell viability and DNA tails are expressed as percentage viability/DNA tail compared with untreated controls. Student's *t*-test was used to determine significance ($p<0.05$).

Cytoplasmic Zn-ion concentration

A549 cells were cultured on 35 mm glass-bottom culture dishes (World Precision Instruments) for live imaging. Cell growth medium was the same as mentioned previously. Prior to imaging, growth medium was removed from dishes, followed by rinsing once with warm imaging buffer (10 mM HEPES at pH 7.4 containing 134.3mM NaCl, 5 mM KCl, 1.2 mM $MgCl_2$, 1.5 mM $CaCl_2$ and 1.44% glucose). 5 μM cell-permanent Zn^{2+} indicator, FluoZin3-AM (Invitrogen), was loaded at 37°C for 45 min. Warm imaging buffer was used twice to wash cells for 15 min at 37 °C each time, so as to remove any dye that was not specifically associated with the cells. ZnO suspensions in imaging buffer were made as described above for the viability and genotoxicity assays. Live imaging was started immediately after addition of ZnO NPs or $ZnCl_2$ (Sigma-Aldrich) using a Delta Vision confocal microscope. A 488 nm wavelength laser was used to excite FluoZin3-AM (EX 494 nm/EM 516 nm). Images were captured from five regions of interest over a period of ~6 h via a 20x objective and each experiment was conducted twice. Fluorescence at each time point was averaged after quantification ($(F-F_0)/F_0$) with ImageJ software, in which F is the fluorescence as a function of time and F_0 at time zero, before addition of ZnO or $ZnCl_2$.

TEM sample preparation

Cell preparation: the ZnO exposed cells (1000 μg/ml; EZ-1 exposed for 1 h, EZ-3 exposed for 6 h) were harvested and placed in fixative (2% glutaraldehyde and 2% formaldehyde in 100 mM PIPES buffer), washed in a buffer, then spun into pellets and fixed in 1% osmium tetroxide. Following dehydration by a series of ascending strength alcohols and washing with dry acetone, the specimens were infiltrated with TAAB resin which was polymerised at 60 ^{o}C

for 24 h. Sections were cut from the polymerised block with a nominal thickness of 90 nm using an ultra-microtome (Leica Ultra-cut E) and placed on a copper grid (Agar Scientific). Both stained (uranyl acetate and lead citrate) and unstained sections were examined by the TEM described previously.

Model Membrane Assays

Lipid vesicle leakage assays and quartz crystal microbalance measurements on solid-supported bilayer systems were conducted as described previously,[25] except that in this study a lipids mixture was used that represents the lipid composition of a typical eukaryotic plasma membrane, but without the sphingomyelin fraction (POPC:DOPE:DOPS:cholesterol in a 9:6:1:4 weight ratio).

Results

Characterisation and dissolution

A range of physico-chemical properties were characterised for all the ZnO NPs under study here (Table 1). TEM was used to determine size and morphology of the samples: for EZ-1 the average near equiaxed particle length is 30±20 nm with the coating not detectable by TEM but identifiable by FTIR as an aliphatic polyether (Supporting Information, Figure S1 and S2); for the uncoated near equiaxed EZ-2, the average particle length is 40±20 nm; and for EZ-3, the average nano-needle size is 1000±500 nm in length and 120±60 nm in width. Powder XRD was used to confirm crystallinity and to indicate (crystalline) phase purity; all samples exhibit the expected zincite phase. DLS measurements revealed NP agglomeration upon dispersion in water and cell culture media, with the uncoated NPs and nano-needles showing significant flocculation, while the polymer coated NPs remain well dispersed. The

zeta potential for the coated NPs when dispersed in water is negative (-14 mV), whereas for the uncoated samples and nano-needles it is positive (5 and 19 mV respectively).

ICP-MS measurement of the soluble zinc supernatant of ZnO NP dispersions in water and cell culture media at NP concentrations of 100 μg/mL (Table 1) indicate levels at the same order of magnitude to those first reported in water by Franklin *et al.*[26] and in media by Song *et al.*[9] We have previously shown that control of pH is absolutely essential, since a decrease of just 0.15 pH units implies a doubling of the free Zn^{2+} concentration of a solution containing non-dissolved ZnO NPs.[7] It is important to note that for sodium bicarbonate buffered cell culture media, like DMEM, small changes in temperature and particularly CO_2 levels can lead to significant changes in solution pH. We have used the electroanalytical method AGNES in order to directly (i.e. without any prior separation steps) measure the free Zn^{2+} concentration produced by the dissolution of the ZnO NPs (EZ-1, EZ-2 and Sigma-Aldrich NPs) when dispersed in DMEM cell culture medium at 37±0.1 ^{o}C and in 5% (±0.2%) CO_2, so that solution pH is controlled to 7.68±0.04 (Figure 1). Sequential additions of $Zn(NO_3)_2$ (Merck) to the DMEM results in a linear rise in Zn^{2+} measured in solution by AGNES (Figure 1). The free Zn^{2+} concentrations are two orders of magnitude lower than the added concentrations of $Zn(NO_3)_2$, indicating a huge complexation capacity of the ligands present in DMEM (amino acids, etc.) for Zn^{2+}. Equilibrium chemical modelling (Visual MINTEQ Version 3.0), consistent with Preis and Gamsjäger,[27] indicated that in DMEM, $ZnCO_3$ (smithsonite) should precipitate when more than 4.5×10^{-7} M 'free', uncomplexed, Zn^{2+} is present. This equilibrium concentration in DMEM is ca. two orders of magnitude below that in equilibrium with bulk ZnO (zincite). However, further additions of $Zn(NO_3)_2$ result in a continued rise of measured free Zn^{2+} in solution, indicating supersaturation (Figure 1; note that one would expect an increase in gradient of the free Zn^{2+} curve if the key

complexing ligands were depleted from the solution at this stage). Importantly, when ZnO NPs are added to the supersaturated solution, a decrease in free Zn^{2+} is observed, down to a value consistent with the concentration in thermodynamic equilibrium with $ZnCO_3$, suggesting that precipitation occurs. A loose, white precipitate different in form to the solid ZnO NPs is indeed visible at this stage and we propose that this is due to the ZnO NPs providing nucleation sites for carbonate precipitation in the supersaturated solution. Additions of ZnO NPs to pristine DMEM solutions result in the formation of similar loose, white precipitates and measured values of free Zn^{2+} that are consistent with the solubility of $ZnCO_3$ and not ZnO (Figure 1).

It is noteworthy that the equilibrium solubility in DMEM estimated by AGNES (5.5 μg ZnO/mL; Figure 1) is in good agreement with the values estimated by ICP-MS (5.1-6.5 μg ZnO/mL; Table 1), despite concerns regarding the overestimation of Zn solubility by ICP-MS.[28] In addition, we have also measured dissolution kinetics by AGNES. At concentrations above 5.5 μg/mL ZnO, uncoated NPs (including EZ-2) typically reach the thermodynamic solubility limit in equilibrium with $ZnCO_3$ within 3-6 h, whereas the coated ZnO NPs (EZ-1) approach this limit only after 48 h incubation (Figure 1, data points labelled with letters and Supplementary Information, Figure S4). In conclusion therefore, the addition of up to 5.5 μg/mL ZnO NPs (70 μM Zn) to DMEM leads to a relatively fast, full dissolution of ZnO NPs, with the majority of the liberated Zn^{2+} ions complexed to organic ligands in the media (only 0.45 μM Zn is 'free' in solution as uncomplexed Zn^{2+}). It is not clear yet whether dispersions of ZnO NPs above this concentration dissolve entirely and re-precipitate as $ZnCO_3$ or whether a $ZnCO_3$ coating of the partially dissolved NPs would result in the retention of some ZnO. Also, the formation of mixed phosphate/carbonate solid phases cannot be excluded from the available data.

Cyto- and genotoxicity

Cytotoxicity of the ZnO NPs and a $ZnSO_4$ solution was tested on two epithelial cell lines after a 24 h incubation period (Figure 2 and Additional File, Table S1). The concentration of $ZnSO_4$ was adjusted to give the same Zn content as used in the assays with ZnO (i.e., $ZnSO_4$ was tested at the same Zn-molarity as ZnO). The cytotoxicity tests gave a wide range of responses, but some general observations can be made. First, the ZnO NPs are no more cytotoxic than the $ZnSO_4$ control. Second, the uncoated, equiaxed NPs (EZ-2) always induced a lower response than the other particles and this NP type was the only one tested to yield median lethal concentration (LC_{50}) values consistently higher than 100 μg/mL for all cell types (Additional File, Table S1). In order to test if the composition of the culture medium had a significant effect, a third cell line was tested. Although HaCaT epithelial cells are typically grown in DMEM media, we have cultured them in RPMI media, which is a more phosphate-rich culture medium than DMEM and could therefore result in re-precipitation of the relatively insoluble, zinc phosphate hydrates, as suggested previously.[4,5] In all but one case, the HaCaT cells incubated in RPMI are more sensitive to ZnO NPs than $ZnSO_4$ suggesting either the different intrinsic sensitivity of these cells compared to the previous model systems, or the different behaviour of zinc in the richer phosphate environment, specifically regarding its possible transformation into other secondary precipitates such as hopeite ($Zn_3(PO_4)_2{:}4H_2O$).

Based on the cytotoxicity results, the three cell lines were treated with ZnO NPs at concentrations up to 10 μg/mL or 1 μg/mL for HaCaT cells (significant cell death at higher concentrations hampers the interpretation of the assay results) to measure the induction of DNA damage using the Comet assay.[29] The results show a small, but significant increase in

DNA damage compared to controls at concentrations of 10 μg/mL ZnO for HT29 cells for the polymer coated NPs (EZ-1) and the uncoated nano-needles (EZ-3; Figure 3). For the HaCaT cells, only the polymer coated NPs (EZ-1) show an increase in DNA damage at 1 μg/mL, while the A549 cells are not significantly affected by any of the NPs (Figure 3).

EZ-2 seems to have a much lower cytotoxicity than EZ-1 or EZ-3 and the Comet assay results suggest this is not due to differences in DNA damage. To study further the mechanism of cytotoxicity, we measured the intracellular Zn^{2+} concentration in A549 cells upon addition of the three NP types. We note that this assay could not be done in DMEM, but is performed in an imaging buffer that does not contain carbonate or phosphate and does contain 1.5 mM $CaCl_2$. As the imaging buffer is devoid of amino acids and other potential soluble Zn ligands, ZnO dissolution should result in much higher 'free' Zn^{2+} in solution; equilibrium solubility of ZnO in the imaging buffer has been measured to be ~20 μg/mL.[7] Correspondingly, cytoplasmic Zn^{2+} concentrations in A549 cells incubated for up to 350 min with the three ZnO NPs at exposure doses of 20 μg/mL do not show a clear rise or distinction between the NPs and a $ZnCl_2$ solution, despite possible perturbation from the high Ca^{2+} concentration (Figure 4). At 1 mg/mL, however, the relative intracellular Zn^{2+} concentrations vary considerably. The uncoated NPs (EZ-2) and $ZnCl_2$ solution both show a sharp rise between 40 and 50 min and then decline by 40%. In contrast, both the polymer coated NPs (EZ-1) and nano-needles (EZ-3) exhibit an almost linear, steady rise of Zn^{2+} up to 350 min (Figure 4). This continuous rise in intracellular Zn^{2+} concentration for the polymer coated ZnO NPs (EZ-1) and uncoated nano-needles (EZ-3) cannot solely be explained by the slower dissolution rates evidenced by AGNES (Figure 1), as the final intracellular Zn^{2+} concentration after 350 min is significantly higher compared to cells incubated with $ZnCl_2$. Instead, we suggest that

at very high NP exposures, EZ-1 and EZ-3 have additional affects due to direct interaction between non-solubilised NPs and the cells.

TEM

In order to determine whether the polymer coated NPs (EZ-1) and uncoated nano-needles (EZ-3) are taken up by cells and if they are, where they localise within the cell, TEM images were recorded for A549 cells incubated with 1 mg/mL ZnO under identical conditions to the viability assay. TEM of the cells incubated with the polymer coated NPs (EZ-1) for 1 h showed that the majority of cells were intact and that ZnO NPs (or possible $ZnCO_3$ particulates) were present in the cytoplasm, albeit partially dissolved (Figure 5). TEM of the cells incubated with nano-needles (EZ-3) for 6 h showed potentially non-viable cells with partially dissolved needles, incompletely internalised (Figure 6).

Model Membrane Interaction

At exposure doses of 1 mg/mL, temporal cytoplasmic Zn^{2+} concentrations suggest that the uncoated, equiaxed ZnO NPs (EZ-2) produce a similar response to $ZnCl_2$ solutions, while the polymer coated NPs (EZ-1) and uncoated nano-needles (EZ-3) follow a different pathway (Figure 4). TEM confirms incomplete cellular internalization for these latter two particle types (Figures 5 and 6). In order to test if either response could be due to a strong interaction between the particles and the plasma membrane, the interaction of the NPs with model membranes was investigated.

First, to study whether the ZnO NPs can cause membrane disruption, vesicle-leakage assays were performed in DMEM. 400-nm diameter unilamellar vesicles composed of POPC:DOPE:DOPS:cholesterol (9:6:1:4 weight ratio) were loaded with an auto-quenching

fluorescent dye and incubated with the NPs. Release of the dye from a vesicle results in a dilution of the fluorescent dye, raising the observed fluorescence intensity. Indeed, significant increases in fluorescence intensity were observed upon addition of all three NP types tested (EZ-1, 2 and 3), indicating some dye is released and the membrane integrity compromised (Figure 7a). Increasing the exposure dose of all three NP types increased the release of dye, however the polymer coated NPs (EZ-1) provoked the highest leakage at all doses and at 100 μg/ml compromised the majority of the vesicles (unlike the other two particle types that induced < 20% leakage at this ZnO dose).

To explore the relatively enhanced ability of the polymer coated NPs (EZ-1) to provoke vesicle leakage, the ability of these particles to bind to a lipid membrane was studied with a Quartz Crystal Microbalance with Dissipation (QCM-D). A tethered bilayer lipid membrane composed of POPC:DOPE:DOPS:cholesterol (9:6:1:4 weight ratio) is formed on silicon-oxide coated QCM-D crystal. After exchanging the buffer for DMEM, binding of NPs on top of the planar lipid membrane was monitored with QCM-D. Upon addition of 10 μg/mL polymer coated NPs (EZ-1), a slight decrease in QCM-D frequency was observed indicating binding to the membrane (Figure 7b). At the same time, the dissipation of the oscillation rose by very little, indicative of a tight interaction between the rigid NPs and the lipid membrane. A larger decrease in frequency and a corresponding small rise in dissipation are observed with the addition of 100 μg/mL. A smaller response is evident for the subsequent addition of 1 mg/mL, suggesting complete coverage of the membrane has been achieved between the two exposure doses. Finally, rinsing the system did not significantly change the frequency or dissipation, suggesting that most of the polymer coated NPs are not released from the membrane and the NPs are bound irreversibly (Figure 7b). Much less binding was observed

for EZ-2 and EZ-3 and all binding was reversible (not shown), suggesting that the coating of EZ-1 enhances interaction with the model membranes and possibly with plasma membranes.

Discussion

It is recognised that much of the toxicity of ZnO NPs is due to the compound's solubility and the release of Zn^{2+} into solution. It is still not clear however, whether observed increases of intracellular Zn^{2+} result from NP dissolution following dispersion in physiological media typically used to culture cells or from cellular uptake of the NPs with subsequent intracellular dissolution and release of Zn^{2+} (for a review see, for instance, Vandebriel and de Jong[10]). We have used well-characterised ZnO NPs (Table 1) to resolve this uncertainty and we conclude that toxic pathways depend on the equilibrium solubility of the ZnO in the dispersion media plus, at relatively high concentrations or short incubation times, the surface coating and morphology of the NPs. We note that our analysis excludes the presence of serum proteins because these are known to interact with ZnO nanoparticles, enhancing membrane activity[30] yet the impact of serum concentration on the amount of cellular uptake and the biological response to the exposure, is not fully understood (see for example[23]).

Up to 5.5 μg/mL of ZnO (70 μM Zn), the particles fully dissolve in DMEM (albeit at a slower rate if polymer coated), while above this concentration, insoluble $ZnCO_3$ (smithsonite) is most likely formed (Figure 1). This stable equilibrium applies to appropriately buffered cell culture media and is in broad agreement with previous work on less well buffered systems. Reed *et al*. used chemical equilibrium modelling to predict the likely re-precipitation of less-soluble zinc hydrocarbonate (hydrozincite) in moderately hard water and zinc phosphate hydrate (hopeite) in the phosphate-rich RPMI cell culture medium.[4] They verified and quantified the formation of re-precipitated particulates in solutions containing EZ-1 amongst

several ZnO NPs tested (as did Turney et al for soluble zinc salts in RPMI[5]). Reed *et al*. also measured the polymer coated ZnO NP (EZ-1) solubility in DMEM (supplemented with bovine serum albumin) and observed similar Zn^{2+} levels in solution to those reported here. However, the pH of their DMEM containing EZ-1 dropped over time and correspondingly, the levels of soluble Zn rose. Such a change in pH would not occur for a cell line buffered in DMEM at 37 ^{o}C and in 5% CO_2 and it is under these conditions that we show a stable equilibrium solubility level equivalent to the complete dissolution of 5.5 μg/mL of ZnO, releasing 67 μM Zn^{2+} of which only 0.45 μM is not complexed to organic ligands and remains free in solution. For DMEM with ZnO concentrations above 5.5 μg/mL, we have not established if the solid fraction of Zn is re-precipitated zinc carbonate (and/or phosphate) particulates, or whether some ZnO NPs are retained with a carbonate coating. Regardless, above the zinc carbonate equilibrium concentration, phase transformed, lower solubility particles will be retained during cellular exposure, consistent with previous observations.[4, 5]

We show that, uncoated, equiaxed ZnO NPs (EZ-2) induce a drop in cell viability at concentrations well above those of $ZnSO_4$ solutions in three different epithelial cell lines (Figure 2 and Supporting Information, Table S1). The higher cytotoxic response of $ZnSO_4$ compared to EZ-2 could be because additions of $ZnSO_4$ can lead to supersaturation of Zn^{2+} with respect to the zinc carbonate equilibrium solubility of DMEM, as has been observed in our solubility experiments (Figure 1). This would imply that the zinc carbonate particulates are less cytotoxic than dissolved Zn^{2+}. Also the polymer coated ZnO NPs and uncoated nano-needles (EZ-1 and 3, respectively) do not exhibit a more acute cytotoxicity than that of $ZnSO_4$ (Figure 2). However, they do provoke a significantly stronger response than EZ-2, suggesting that the coating and the morphology affect cytotoxicity. EZ-1 and EZ-3 are able to induce a steady rise in intracellular Zn^{2+} to concentrations above that of EZ-2 or $ZnSO_4$

(Figure 4). TEM confirms the cellular uptake of partially dissolved, polymer coated ZnO NPs and uncoated nano-needles (Figures 5 and 6, respectively). The nano-needles (EZ-3) readily flocculate upon dispersion in cell culture media (Table 1) such that sedimentation and rapid contact with cell membranes will occur during exposure but even so, they are incompletely internalised (Figure 6). We suggest that this incomplete or frustrated cellular uptake contributes to the acute cell viability response (Figure 2); uptake of ZnO nano-needles has been shown in human macrophage monocyte cells[13] but A549 cells are not normally phagocytic and may struggle to complete endocytic internalisation of such large needle agglomerates (Table 1). Frustrated cellular uptake is an established phenomenon for fibres in general.[31] Endocytic cellular uptake of the polymer coated ZnO NPs (EZ-1) however, does not appear to be frustrated (Figure 5) and is consistent with the slower dissolution rate of these NPs (Figure 1 and Figure S4). Additional experiments with model membranes confirm that EZ-1 binds to lipid membranes, possibly promoting endocytic uptake and raising intracellular Zn^{2+} (Figure 7). Alternatively, our vesicle leakage assay shows that EZ-1 has a disrupting effect on the membrane, thus it cannot be excluded that EZ-1 compromises the plasma membrane, thereby allowing ZnO and Zn^{2+} to passively enter the cell. It is currently not clear whether the aliphatic polyether polymer coat of EZ-1 is responsible for disrupting the lipid or whether a stable colloid suspension of ZnO is more damaging than agglomerates of ZnO/$ZnCO_3$ NPs. It has been shown recently however that the lipid membrane activity of ZnO NPs is enhanced in the presence of serum albumin because it forms a protein corona around the NPs.[30] It could be that the protein corona and aliphatic polyether polymer coating of EZ-1 have a common physical mechanism by which they impair the integrity of a lipid membrane.

Ultimately, it may be that exposing ZnO NPs to CO_2 rich atmospheres during the manufacture of ZnO NP products, to develop a $ZnCO_3$ coating, could mitigate much of the toxicity reported thus far. Obviously, any coating would have to not interfere significantly with the original performance properties of the NPs.

Conclusions

Overall, our data indicate the importance of understanding the role of the content of cell culture media used for testing the toxicity of ZnO NPs to cell lines *in vitro*. Cell viability (and induced DNA damage) depends on the equilibrium solubility of ZnO in the culture media (5.5 μg/mL ZnO or 67 μM Zn for dispersions in DMEM, held at pH 7.68). At NP concentrations well above the equilibrium solubility limit, ZnO NP morphology and surface coating are also factors. Polymer coatings that slow dissolution but promote strong interaction with lipid membranes will enhance the toxicity of ZnO NPs through increased cellular uptake followed by intracellular dissolution. In order to limit toxicity, surface coatings that prevent dissolution in these media, maintain NP dispersion and do not enhance interactions with cellular membranes should be sought. Similarly, needle-like morphologies also enhance the toxicity of ZnO NPs at high concentrations, by apparently frustrating cellular uptake. Thus, ZnO NP synthesis that avoids producing acicular morphologies is recommended.

Acknowledgements

The work leading to these results has received funding from the European Union Seventh Framework Programme (FP7-NMP-2008-1.3-2) under grant agreement n° 229244. APB holds an EPSRC ARF (EP/E059678/1). CAD, JG and CRC also received support from the European Union Seventh Framework Programme (FP7-NMP.2012.1.3-3) under grant agreement nº 310584 (NANoREG). None of the funding sources have been involved in the

study design; in the collection, analysis and interpretation of data; in the writing of the report; or in the decision to submit the paper for publication. We thank Prof. Alice Warley of the Centre for Ultrastructural Imaging, King's College London for enabling the preparation of thin sections for TEM.

Supporting Information Available

Supporting Information is available free of charge via the Internet at http://pubs.acs.org.

References

(1) Lombi, E., Donner, E., Tavakkoli, E., Turney, T. W., Naidu, R., Miller, B. W., and Scheckel, K. G. (**2012**) Fate of zinc oxide nanoparticles during anaerobic digestion of wastewater and post-treatment processing of sewage sludge. *Environ. Sci. Technol.* 46, 9089-9096.

(2) Lv, J. T., Zhang, S. Z., Luo, L., Han, W., Zhang, J., Yang, K., and Christie, P. (**2012**) Dissolution and microstructural transformation of ZnO nanoparticles under the influence of phosphate. *Environ. Sci. Technol.* 46, 7215-7221.

(3) Ma, R., Levard, C., Michel, F. M., Brown, G. E., and Lowry, G. V. (**2013**) Sulfidation mechanism for zinc oxide nanoparticles and the effect of sulfidation on their solubility. *Environ. Sci. Technol.* 47, 2527-2534.

(4) Reed, R. B., Ladner, D. A., Higgins, C. P., Westerhoff, P., and Ranville, J. F. (**2012**) Solubility of nano-zinc oxide in environmentally and biologically important matrices. *Environ. Toxicol. Chem.* 31, 93-99.

(5) Turney, T. W., Duriska, M. B., Jayaratne, V., Elbaz, A., O'Keefe, S. J., Hastings, A. S., Piva, T. J., Wright, P. F. A., and Feltis, B. N. (**2012**) Formation of zinc-containing nanoparticles from Zn^{2+} ions in cell culture media: Implications for the nanotoxicology of ZnO. *Chem. Res. Toxicol.* 25, 2057-2066.

(6) Adam, N., Schmitt, C., Galceran, J., Companys, E., Vakourov, A., Wallace, R., Knapen, D., and Blust, R. (**2014**) The chronic toxicity of ZnO nanoparticles and $ZnCl_2$ to *Daphnia magna* and the use of different methods to assess nanoparticle aggregation and dissolution. *Nanotoxicology* 8, 709-717.

(7) David, C. A., Galceran, J., Rey-Castro, C., Puy, J., Companys, E., Salvador, J., Monne, J., Wallace, R., and Vakourov, A. (**2012**) Dissolution kinetics and solubility of ZnO nanoparticles followed by AGNES. *J. Phys. Chem. C* 116, 11758-11767.

(8) Xia, T., Kovochich, M., Liong, M., Madler, L., Gilbert, B., Shi, H. B., Yeh, J. I., Zink, J. I., and Nel, A. E. (**2008**) Comparison of the mechanism of toxicity of zinc oxide and cerium oxide nanoparticles based on dissolution and oxidative stress properties. *ACS Nano* 2, 2121-2134.

(9) Song, W. H., Zhang, J. Y., Guo, J., Zhang, J. H., Ding, F., Li, L. Y., and Sun, Z. T. (**2010**) Role of the dissolved zinc ion and reactive oxygen species in cytotoxicity of ZnO nanoparticles. *Toxicol. Lett.* 199, 389-397.

(10) Vandebriel, R. J., and De Jong, H. J. (**2012**) A review of mammalian toxicity of ZnO nanoparticles. *Nanotechnology, Science and Applications* 5, 61-71.

(11) Lin, W. S., Xu, Y., Huang, C. C., Ma, Y. F., Shannon, K. B., Chen, D. R., and Huang, Y. W. (**2009**) Toxicity of nano- and micro-sized ZnO particles in human lung epithelial cells. *J. Nanopart. Res.* 11, 25-39.

(12) Fukui, H., Horie, M., Endoh, S., Kato, H., Fujita, K., Nishio, K., Komaba, L. K., Maru, J., Miyauhi, A., Nakamura, A., Kinugasa, S., Yoshida, Y., Hagihara, Y., and Iwahashi, H. (**2012**) Association of zinc ion release and oxidative stress induced by intratracheal instillation of ZnO nanoparticles to rat lung. *Chem-Biol. Interact.* 198, 29-37.

(13) Muller, K. H., Kulkarni, J., Motskin, M., Goode, A., Winship, P., Skepper, J. N., Ryan, M. P., and Porter, A. E. (**2010**) pH-Dependent toxicity of high aspect ratio ZnO nanowires in macrophages due to intracellular dissolution. *ACS Nano* 4, 6767-6779.

(14) Gilbert, B., Fakra, S. C., Xia, T., Pokhrel, S., Madler, L., and Nel, A. E. (**2012**) The fate of ZnO nanoparticles administered to human bronchial epithelial cells. *ACS Nano* 6, 4921-4930.

(15) Moos, P. J., Chung, K., Woessner, D., Honeggar, M., Cutler, N. S., and Veranth, J. M. (**2010**) ZnO particulate matter requires cell contact for toxicity in human colon cancer cells. *Chem Res Toxicol* 23, 733-739.
(16) Cho, W. S., Duffin, R., Howie, S. E., Scotton, C. J., Wallace, W. A., Macnee, W., Bradley, M., Megson, I. L., and Donaldson, K. (**2011**) Progressive severe lung injury by zinc oxide nanoparticles; the role of Zn^{2+} dissolution inside lysosomes. *Particle Fibre Toxicol.* 8, 27.
(17) Sharma, V., Singh, P., Pandey, A. K., and Dhawan, A. (**2012**) Induction of oxidative stress, DNA damage and apoptosis in mouse liver after sub-acute oral exposure to zinc oxide nanoparticles. *Mutat. Res.-Gen. Tox. En.* 745, 84-91.
(18) Handy, R. D., Cornelis, G., Fernandes, T., Tsyusko, O., Decho, A., Sabo-Attwood, T., Metcalfe, C., Steevens, J. A., Klaine, S. J., Koelmans, A. A., and Horne, N. (**2012**) Ecotoxicity test methods for engineered nanomaterials: Practical experiences and recommendations from the bench. *Environ. Toxicol. Chem.* 31, 15-31.
(19) Krug, H. F., and Wick, P. (**2011**) Nanotoxicology: An interdisciplinary challenge. *Angew. Chem. Int. Ed.* 50, 1260-1278.
(20) Kunzmann, A., Andersson, B., Thurnherr, T., Krug, H., Scheynius, A., and Fadeel, B. (**2011**) Toxicology of engineered nanomaterials: Focus on biocompatibility, biodistribution and biodegradation. *BBA-Gen. Subjects* 1810, 361-373.
(21) Dhawan, A., and Sharma, V. (**2010**) Toxicity assessment of nanomaterials: Methods and challenges. *Anal. Bioanal. Chem.* 398, 589-605.
(22) Elsaesser, A., and Howard, C. V. (**2012**) Toxicology of nanoparticles. *Adv. Drug Delivery Rev.* 64, 129-137.
(23) Doak, S. H., Griffiths, S. M., Manshian, B., Singh, N., Williams, P. M., Brown, A. P., and Jenkins, G. J. S. (**2009**) Confounding experimental considerations in nanogenotoxicology. *Mutagenesis* 24, 285-293.
(24) Galceran, J., Companys, E., Puy, J., Cecilia, J., and Garces, J. L. (**2004**) AGNES: a new electroanalytical technique for measuring free metal ion concentration. *J. Electroanal. Chem.* 566, 95-109.
(25) Mu, Q. S., Hondow, N. S., Krzeminski, L., Brown, A. P., Jeuken, L. J. C., and Routledge, M. N. (**2012**) Mechanism of cellular uptake of genotoxic silica nanoparticles. *Particle Fibre Toxicol.* 9, 29.
(26) Franklin, N. M., Rogers, N. J., Apte, S. C., Batley, G. E., Gadd, G. E., and Casey, P. S. (**2007**) Comparative toxicity of nanoparticulate ZnO, bulk ZnO, and $ZnCl_2$ to a freshwater microalga (*Pseudokirchneriella subcapitata*): The importance of particle solubility. *Environ. Sci.Technol.* 41, 8484-8490.
(27) Preis, W., and Gamsjäger, H. (**2001**) (Solid + solute) phase equilibria in aqueous solution. XIII. Thermodynamic properties of hydrozincite and predominance diagrams for (Zn^{2+} + H_20 + CO_2). *J. Chem. Thermodynamics* 33, 803-819.
(28) Xu, M., Li, J., Hanagata, N., Su, H., Chen, H., and Fujita, D. (**2013**) Challenge to assess the toxic contribution of metal cation released from nanomaterials for nanotoxicology - the case of ZnO nanoparticles. *Nanoscale* 5, 4763-4769.
(29) Hillegass, J. M., Shukla, A., Lathrop, S. A., MacPherson, M. B., Fukagawa, N. K., and Mossman, B. T. (**2010**) Assessing nanotoxicity in cells *in vitro*. *WIREs-Nanomed. Nanobiotechnol.* 2, 219-231.
(30) Churchman, A. H., Wallace, R., Milne, S. J., Brown, A. P., Brydson, R., and Beales, P. A. (**2013**) Serum albumin enhances the membrane activity of ZnO nanoparticles. *Chem. Commun.* 49, 4172-4174.
(31) Murphy, F. A., Schinwald, A., Poland, C. A., and Donaldson, K. (**2012**) The mechanism of pleural inflammation by long carbon nanotubes: Interaction of long

fibres with macrophages stimulates them to amplify pro-inflammatory responses in mesothelial cells. *Particle Fibre Toxicol.* 9, 8.

Table 1: Physico-chemical properties of the three ZnO NPs

	EZ-1	EZ-2	EZ-3
Name	Aliphatic Polyether Coated[a] NPs	Uncoated NPs	Uncoated Nano-needles
Source	Alpha Aesar 45409	Alpha Aesar 44533	In-house
TEM	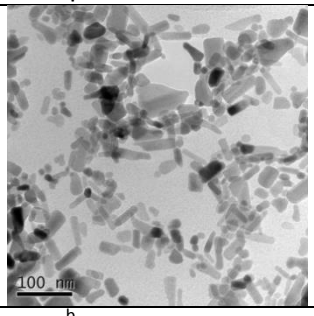	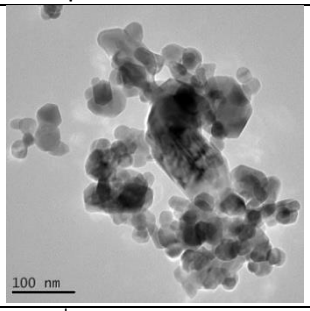	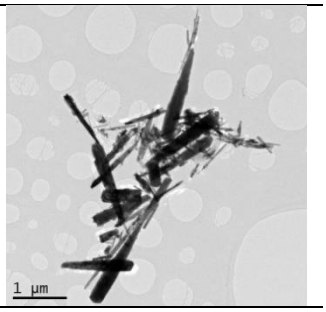
Particle size	[b]L = 30 ± 20 nm W = 16 ± 10 nm FR = 1.9 ± 0.8	[b]L = 40 ± 20 nm W = 30 ± 12 nm FR = 1.5 ± 0.3	[c]L = 1024 ± 496 nm W = 115 ± 59 nm FR = 9.8 ± 4.4
XRD	Consistent with zincite (01-071-6424) = hexagonal phase		
Hydrodynamic diameter water[d]	70-150 nm Stable	90-160 nm 390-670 nm Unstable	250-540 nm 2520-3030 nm Unstable
Hydrodynamic diameter media[d]	40-140 nm Stable	1330-2150 nm Unstable	[e]180-1590 nm 2520-3050nm Very unstable
Zeta potential[f]	-14 ± 6 mV	5 ± 5 mV	19 ± 5 mV
Dissolved ZnO in water by ICP-MS [g]	1.73 ± 0.03 µg/mL	1.19 ± 0.03 µg/mL	NA
Dissolved ZnO in medium by ICP-MS [g]	6.5 ± 0.2 µg/mL	5.1 ± 0.1 µg/mL	[h]16.5 µg/mL
Dissolved ZnO in medium by AGNES	5.5± 0.7 [i]µg/mL	5.5±0.7[i] µg/mL	NA

[a]Coating type is unreported by manufacturer however FTIR indicates it to be an aliphatic polyether. Primary particle size measured from [b]250 particles and [c]109 nano-needles in TEM images (FR = Feret ratio). [d]Hydrodynamic diameters measured in water at 25 °C at 1000 µg/mL and in media at 37 °C and 100 µg/mL, except [e] measured at 37 °C and 1000 µg/mL. [f]Zeta potential measured in water, with errors from FWHM. [g]ICP-MS conducted on supernatants from ZnO dispersions in DMEM at 37 °C and 100 µg/mL. [h]in RPMI, [i]at 95% confidence level, estimated from AGNES measurements and free Zn^{2+} concentration expected in equilibrium with $ZnCO_3$.

Figure Legends

Figure 1: Free Zn^{2+} concentration after addition of Zn(II) salt solutions or ZnO NPs to DMEM at 37.0 ºC under 5% CO_2/ 95% N_2 atmosphere with pH = 7.68. Markers: $Zn(NO_3)_2$ (*plus signs*); uncoated Sigma-Aldrich ZnO (*open circles*); uncoated EZ-2 particles (*diamonds*); coated EZ-1 particles (*filled circles*). The letter by the markers denotes the incubation time in DMEM: a) 30 min; b) 2 h; c) 18-24 h; d) 48 h. The values measured with $Zn(NO_3)_2$ (*plus signs*) remained constant for at least 6 h. The red and blue dashed lines denote the free Zn^{2+} concentration in equilibrium with solid $ZnCO_3$ (smithsonite) and ZnO (zincite) bulk phases, respectively, as calculated with Visual MINTEQ (Version 3.0). Note the logarithmic scale of all axes, where concentration units are expressed in mol/L (left and bottom) and its equivalence in μg ZnO/mL (right and top). The zinc carbonate equilibrium solubility level is equivalent to the complete dissolution of 5.5 μg/mL of ZnO in this medium.

Figure 2: Viability of A549, HT29 and HaCaT cells after 24 h incubation with a range of concentrations of ZnO nanoparticle types, EZ-1, -2 and -3 as indicated. Responses to $ZnSO_4$ solutions are also included. Asterisks indicate significance with * for $p<0.05$; ** for $p<0.01$ and *** for $p<0.001$.

Figure 3: DNA strand breaks in A549, HT29 and HaCaT cells following 24 h incubation with a range of concentrations of the three ZnO NP types as determined by the Comet assay (the 0.1 μg/mL concentration of EZ-2 was not tested). Asterisks indicate significance with * for $p<0.05$; ** for $p<0.01$ and *** for $p<0.001$.

Figure 4: Cytoplasmic Zn concentration of A549 cells as a function of time after addition of the three different ZnO NP types and $ZnCl_2$ at a concentration of either 20 μg/mL (*open symbols*) or 1 mg/mL (*closed symbols*). Zn concentration was measured with the fluorescent dye FluoZin3-AM and fluorescence intensity is given as $(F - F_0)/(F_0)$, where F_0 is the intensity at time zero and F the intensity at the indicated time. Error bars indicate the range (standard deviations) of fluorescence measurements at each time point.

Figure 5: **A**: TEM images of an A549 cell after 1 h incubation at 37ºC with 1 mg/mL of the polymer coated NPs (EZ-1); section is not stained with heavy metals. **B**: An enlargement of the dashed square shown in image (A). **C**: Enlargement of the dashed square in (B) showing

ZnO NPs encapsulated within the cytoplasm (note the porous, partially dissolved morphology of the NPs). **D**: EDX spectrum of the area in image (C) confirming the ZnO composition (above background) of the NPs (Os decorates lipid membranes following fixation and the Cu background is generated by the TEM support grid).

Figure 6: **A**: TEM images of two A549 cells after 6 h incubation at 37ºC with 1 mg/mL of nano-needles (EZ-3); section is stained with heavy metals (U and Pb) for image contrast. **B** and **C**: Enlargements of the dashed squares shown in image, with the regions of intact membrane marked in red (A). Note the incomplete internalization of the needles and their porous, partially dissolved morphology. **D**: EDX spectrum of the area in image (C) confirming the ZnO composition (above background) of the needle relics (with additional signals from the heavy metal stains).

Figure 7: **A**: Leakage of carboxyfluorescein (CF) from CF-loaded (50 mM) vesicles in DMEM after the addition of 1, 10, 20 and 100 μg/mL of the three ZnO NPs, as indicated. Leakage was determined from the fluorescence intensity of CF with 0% leakage taken as the fluorescence prior to addition of ZnO NPs and 100% leakage is defined as the fluorescence measure after addition of 1% Triton X-100. The vesicles (~ 400 nm) are made up from POPC:DOPE:DOPS:cholesterol (9:6:1:4 weight ratio). **B**: Adsorption of the polymer coated NPs (EZ-1) on to a solid-supported bilayer lipid membrane (sBLM) as measured with quartz-crystal microbalance with dissipation (frequency – *bottom*; dissipation – *top*). The formation of the sBLM (between 0 and 50 min) from vesicles containing POPC:DOPE:DOPS:cholesterol (9:6:1:4 weight ratio) is not shown for clarity. Arrows indicate additions to the DMEM stock solution of increasing concentrations of NPs, followed by a final rinse with DMEM.

Figures

Figure 1

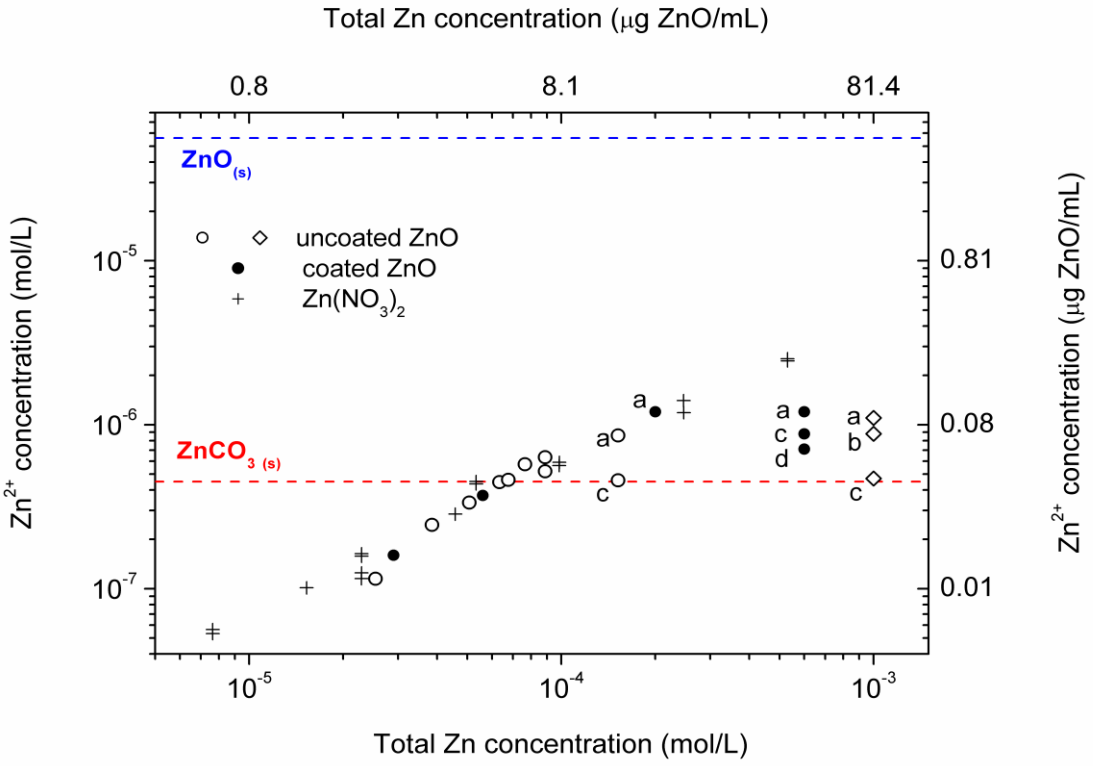

Figure 2

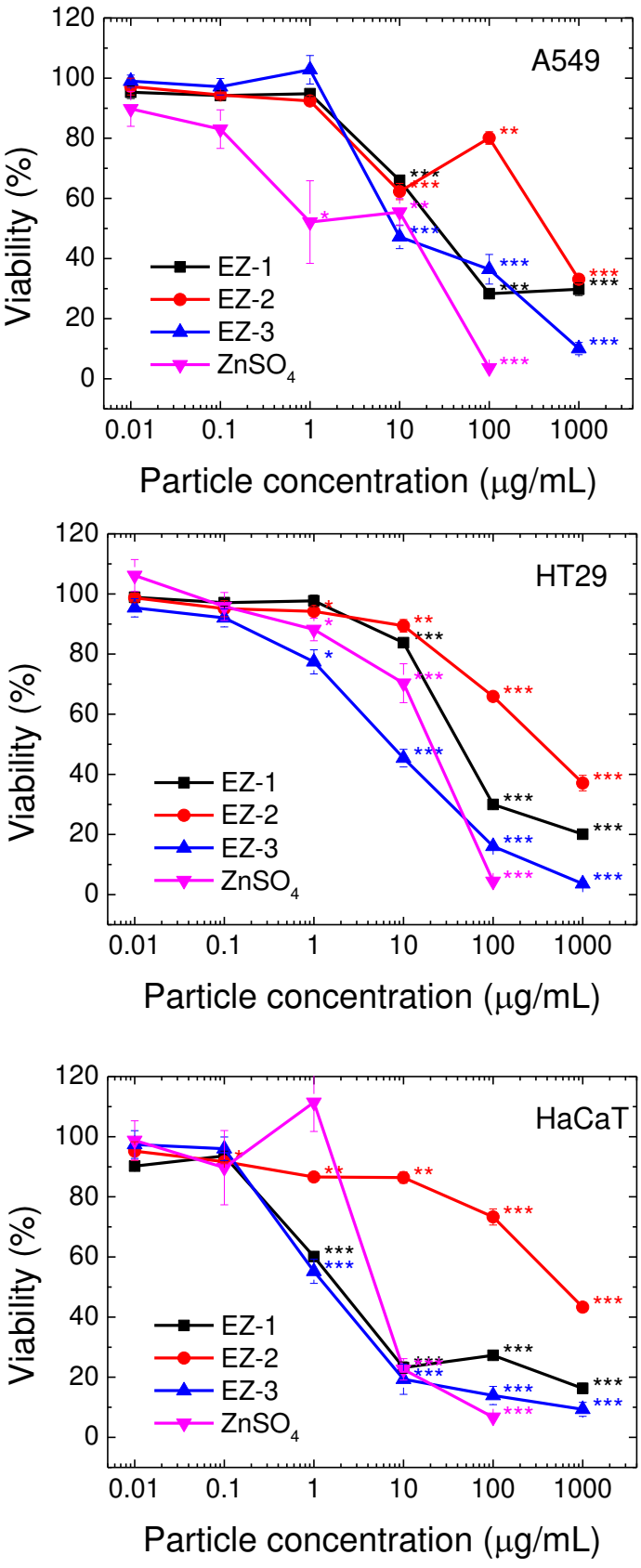
A549
HT29
HaCaT
Viability (%)
Particle concentration (μg/mL)
EZ-1
EZ-2
EZ-3
ZnSO4
0
20
40
60
80
100
120
0.01
0.1
1
10
100
1000
*
**
***

Figure 3

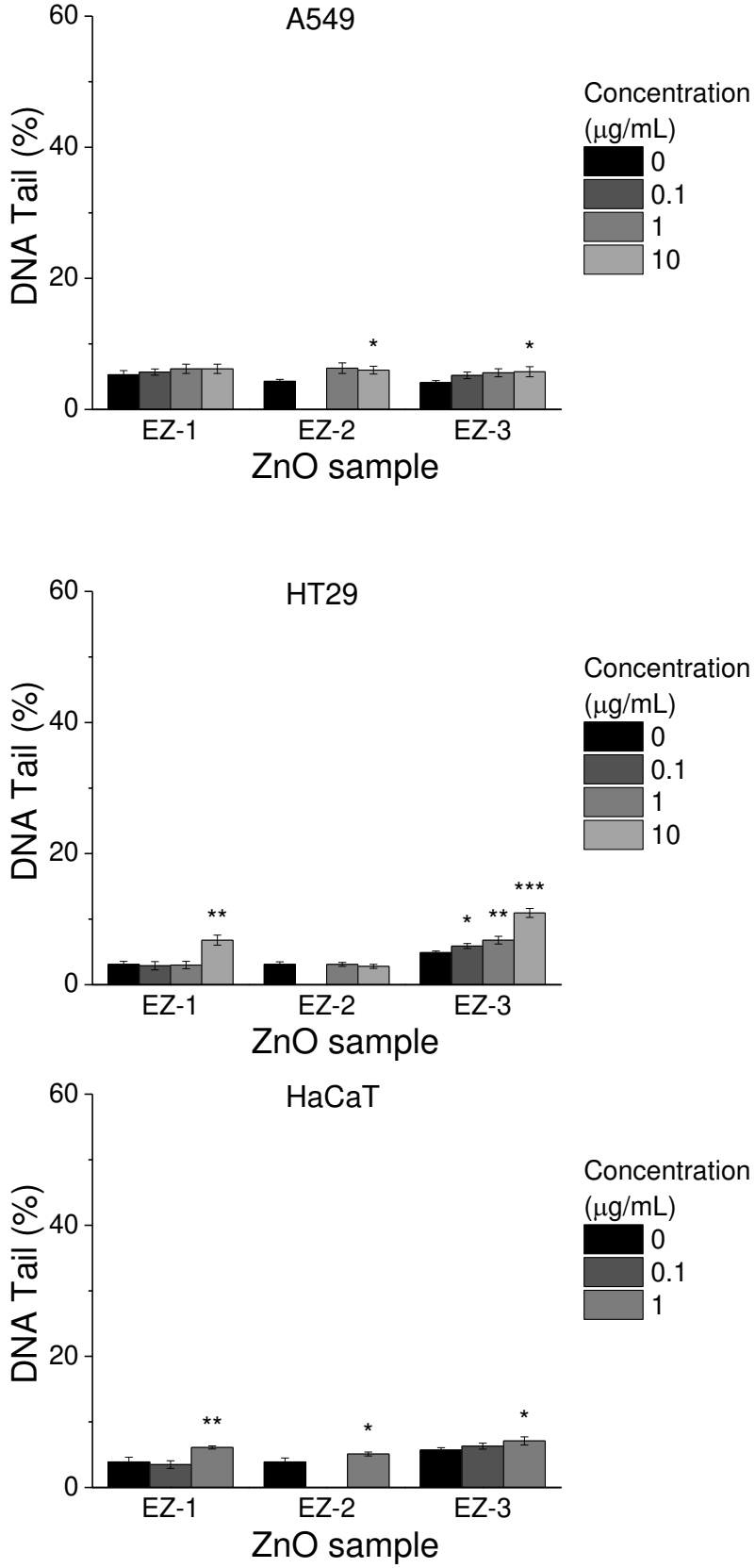
A549
DNA Tail (%)
60
40
20
0
EZ-1
EZ-2
EZ-3
ZnO sample
Concentration
(μg/mL)
0
0.1
1
10
*
*
HT29
DNA Tail (%)
60
40
20
0
EZ-1
EZ-2
EZ-3
ZnO sample
Concentration
(μg/mL)
0
0.1
1
10
**
*
**
***
HaCaT
DNA Tail (%)
60
40
20
0
EZ-1
EZ-2
EZ-3
ZnO sample
Concentration
(μg/mL)
0
0.1
1
**
*
*

Figure 4

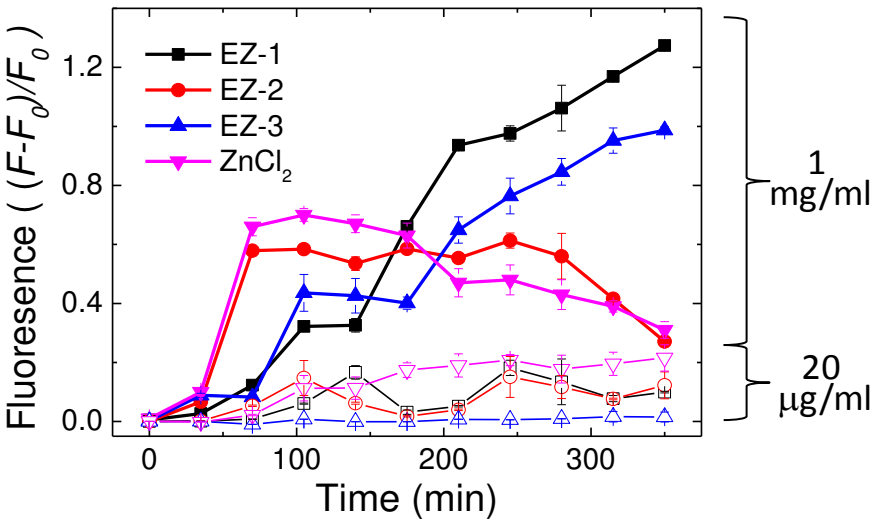
EZ-1
EZ-2
EZ-3
ZnCl2
Fluoresence ((F-F0)/F0)
1.2
0.8
0.4
0.0
0
100
200
300
Time (min)
1
mg/ml
20
μg/ml

Figure 5

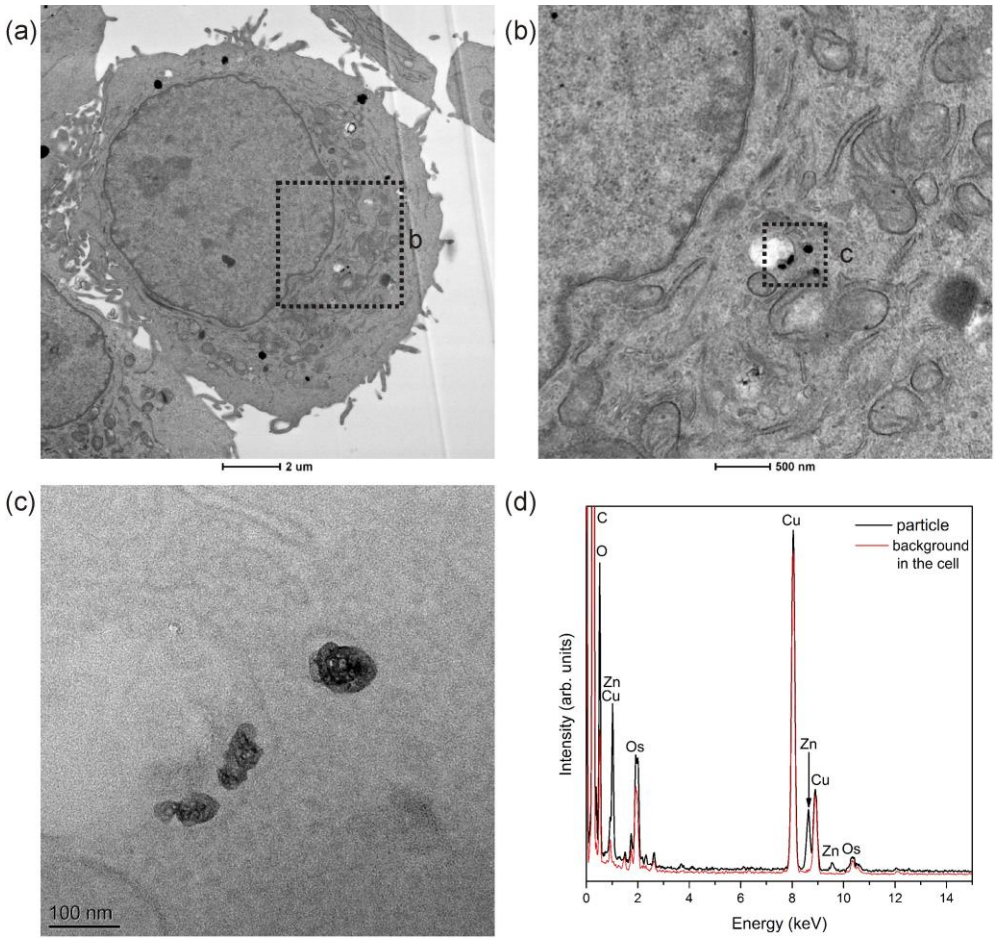
(a)
b
2 um
(b)
c
500 nm
(c)
100 nm
(d)
C
O
Zn
Cu
Os
Cu
Zn
Cu
Zn
Os
particle
background
in the cell
Intensity (arb. units)
0
2
4
6
8
10
12
14
Energy (keV)

Figure 6

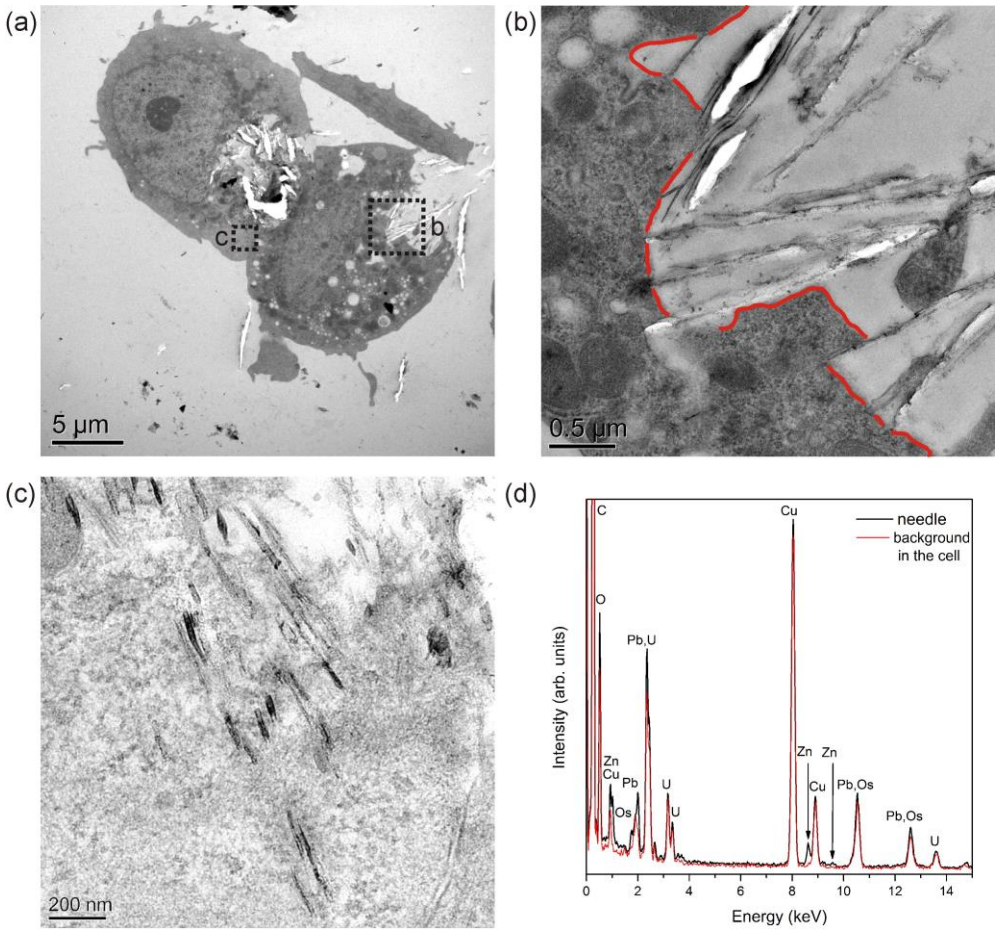
(a)
c
b
5 µm
(b)
0.5 µm
(c)
200 nm
(d)
C
O
Zn
Cu
Pb
Os
Pb,U
U
Cu
Zn
Cu
Zn
Pb,Os
Pb,Os
U
needle
background
in the cell
Intensity (arb. units)
0
2
4
6
8
10
12
14
Energy (keV)

Figure 7

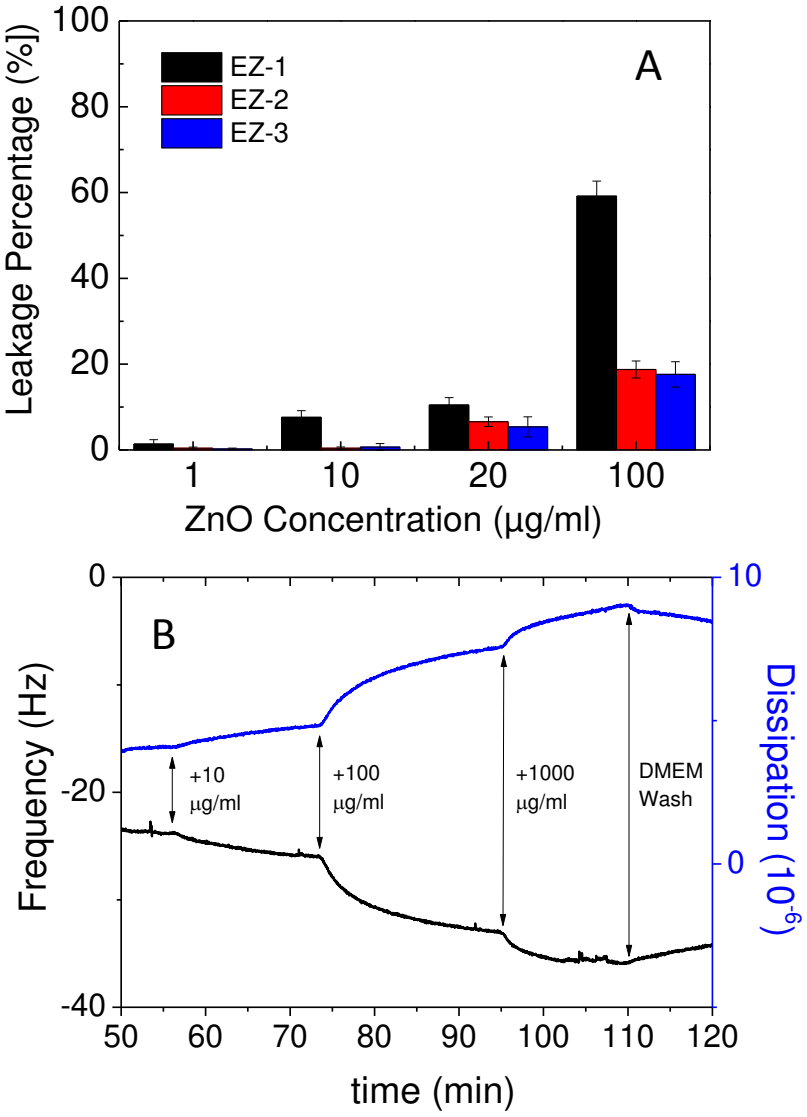
A
EZ-1
EZ-2
EZ-3
Leakage Percentage (%])
ZnO Concentration (µg/ml)
B
Frequency (Hz)
Dissipation (10^{-6})
+10 µg/ml
+100 µg/ml
+1000 µg/ml
DMEM Wash
time (min)